Ferroelectric Materials

Deutsche Ausgabe: DOI: 10.1002/ange.201606079
Internationale Ausgabe: DOI: 10.1002/anie.201606079

Exploring a Lead-free Semiconducting Hybrid Ferroelectric with a Zero-Dimensional Perovskite-like Structure

Zhihua Sun[+], Aurang Zeb[+], Sijie Liu, Chengmin Ji, Tariq Khan, Lina Li, Maochun Hong, and Junhua Luo**

Abstract: *Perovskite lead halides ($CH_3NH_3PbI_3$) have recently taken a promising position in photovoltaics and optoelectronics because of remarkable semiconducting properties and possible ferroelectricity. However, the potential toxicity of lead arouses great environmental concern for widespread application. A new chemically tailored lead-free semiconducting hybrid ferroelectric is reported, N-methylpyrrolidinium)$_3Sb_2Br_9$ (**1**), which consists of a zero-dimensional (0-D) perovskite-like anionic framework connected by corner-sharing $SbBr_6$ coordinated octahedra. It presents a large ferroelectric spontaneous polarization of approximately 7.6 $\mu C\,cm^{-2}$, as well as notable semiconducting properties, including positive temperature-dependent conductivity and ultraviolet-sensitive photoconductivity. Theoretical analysis of electronic structure and energy gap discloses a dominant contribution of the 0-D perovskite-like structure to the semiconducting properties of the material. This finding throws light on the rational design of new perovskite-like hybrids, especially lead-free semiconducting ferroelectrics.*

Hybrid perovskite materials have promoted rapid progress of photoelectronics and photovoltaics over the last decade, including electroluminescent devices,[1] thin-film field-effect transistors,[2] and solar cells.[3] These materials benefit from structural flexibility and tunability of their assemblies, which are constructed from inorganic and/or organic building blocks, leading to prominent semiconducting attributes, such as high charge-carrier mobility and long diffusion length.[4] For instance, organometal trihalide perovskites of $CH_3NH_3PbI_3$ and its derivates have been reported to exhibit long range electron–hole diffusion lengths exceeding 175 μm,[5] which is responsible for extremely high power conversion efficiencies (larger than 20%) in perovskite-based solar cells. Moreover, ferroelectric activities were also proposed to facilitate highly effective photoconversion.[6] Taking $CH_3NH_3PbI_3$ as an example, a large electronic polarization of approximately 38 $\mu C\,cm^{-2}$ has been predicted by some theoretical calculations.[7] It was deemed that such strong polarizations would create an extremely high built-in electric field, and further enhance the separation of charge carriers and concomitantly improve the charge-carrier lifetimes.[8] For this reason researchers have tried to explicate the photoelectric performances of lead-trihalide perovskites based on ferroelectric polarization.[9] However, although theoretical analysis has predicted strong ferroelectric polarization for $CH_3NH_3PbI_3$, up to now there is no conclusive evidence for its bulk ferroelectricity. In this context, the rational design of perovskite-type hybrid ferroelectrics with semiconducting properties, which combine ferroelectricity and other striking optoelectric properties,[10] still remains a great challenge.

Structurally, it is essential that the requirements of ion-size constraints are fulfilled to achieve design of the three-dimensional (3-D) hybrid perovskites of AMX_3 (where A = organic cation, M = metal, and X = halogen). The dimensionality here mainly involves the connectivity of corner-sharing MX_6 octahedra, and the tolerance factor for ion size represents a great constraint to 3-D perovskite structures.[11] For instance, the corner-sharing network of PbI_6 octahedra in $CH_3NH_3PbI_3$ dictates that small $CH_3NH_3^+$ cations occupy 12-fold coordinated holes, while the ethylammonium cation cannot fulfill the same space-filling condition.[12] This suggests that a delicate balance should be achieved between the cation (A) and framework (MX_6) to construct 3-D perovskites. Alternatively, lower-dimensional perovskite hybrids have been widely explored, deriving from the parent 3-D structure down to the isolated 0-D octahedral cluster.[13] In particular, the MX_6 octahedra of isolated 0-D derivatives enables shifting of the positions of octahedra relative to one another, breaking through the ion-size constraints. For example, in 0-D perovskite-derived hybrids of $A_3M_2X_9$ ($M = Sb^{3+}$ and Bi^{3+}), the stereochemically active lone-pair s^2 electrons on M^{3+} lead to structural distortions of the MX_6 network. Such a dynamic feature leads to large freedom of motions and greatly favors the generation of ferroelectricity. Moreover, the trivalent antimony ion is isoelectronic with Sn^{2+} and Pb^{2+},[14] and electronegativities and ionic radii of these elements are similar. Thus, Sb^{III}-based perovskite halides are expected to exhibit comparable semiconducting behaviors with Pb^{II}-based hybrids. That is, Sb^{III}-based perovskite halides have the potential to undertake a key role in constructing new ferroelectric matetrials with semiconducting properties.

[*] Dr. Z. Sun,[+] C. Ji, Dr. L. Li, Prof. M. Hong, Prof. J. Luo
State Key Laboratory of Structural Chemistry, Fujian Institute of Research on the Structure of Matter, Chinese Academy of Sciences
Fuzhou, Fujian, 350002 (P.R. China)
and
Key Laboratory of Optoelectronic Materials Chemistry and Physics
Fujian Institute of Research on the Structure of Matter
Chinese Academy of Sciences
Fuzhou, Fujian, 350002 (P.R. China)
E-mail: sunzhihua@fjirsm.ac.cn
jhluo@fjirsm.ac.cn
A. Zeb,[+] S. Liu, T. Khan
University of the Chinese Academy of Sciences
Beijing 100039 (P.R. China)
[+] These authors contributed equally to this work.

Supporting information for this article can be found under: http://dx.doi.org/10.1002/anie.201606079.

Herein, we demonstrate a new lead-free hybrid ferroelectric, (*N*-methylpyrrolidinium)$_3$Sb$_2$Br$_9$ (**1**), in which the corner-sharing $SbBr_6$ octahedral clusters construct a 0-D perovskite-like anionic framework. The coordinated distortion of $SbBr_6$ octahedra and order–disorder of organic cations lead to a large ferroelectric polarization of about 7.6 $\mu C\,cm^{-2}$. Interestingly, **1** also exhibits notable semiconducting properties, including positive temperature-dependent conductivity and ultraviolet-sensitive photoconductivity. The 0-D inorganic $[Sb_2Br_9]^{3-}$ clusters make a dominant contribution to charge transport in **1**, resembling that of tin- and lead-based perovskites. To our best knowledge, **1** is a new lead-free ferroelectric, featuring a 0-D perovskite-like structure. This finding opens up possibilities for further design of new perovskite hybrids, especially lead-free semiconducting ferroelectrics.

Compound **1** was prepared from aqueous solutions as bulk crystals, with a size up to $5\times4\times3\ mm^3$, and the purity was confirmed by powder X-ray diffraction (Supporting Information, Figures S1 and S2). Structural analyses reveal that **1** belongs to the trigonal system with a polar space group of *R*3*c* at 293 K (Supporting Information, Table S1). Its basic unit contains a discrete inorganic cluster of $[Sb_2Br_9]^{3-}$ and three equivalent organic *N*-methylpyrrolidinium cations. The central antimony atoms of $[Sb_2Br_9]^{3-}$ dimers are coordinated by six bromide atoms, three of which behave as bridging linkers (Figure 1 a). It is noteworthy that the geometry of this structural bioctahedron is slightly distorted, as deduced from the disparity between Sb–Br bond lengths. For instance, bond lengths of Sb_1–Br_1 and Sb_1–Br_3 are 2.604 and 3.114 Å, while the values for Sb_2–Br_2 and Sb_2–Br_3 are 2.607 and 3.129 Å. Such differences support the observation that two adjacent octahedra have distinctly asymmetric configurations, induced by shifts or relative motions of bridging bromide atoms. The coordinated distortion can also be confirmed from the Br-Sb-Br bond angles of the $SbBr_6$ building blocks, which form an irregular architecture. Such a distorted configuration for the inorganic moieties of **1** is quite similar to other hybrids, such as $[(CH_3)_4P]_3Bi_2Br_9$ and $[(CH_3)_4N]_3Sb_2Cl_9$.[15] For these analogues, the $<111>$ oriented perovskite-derived structure, featuring $M_2X_9^{3-}$ dimers of two MX_6 face-sharing octahedra, is created by excising along the [111] direction of the 3-D parent prototype. This topology is described as a 0-D perovskite structure, based on the connectivity of corner-sharing MX_6 octahedra.[16] In this regard, **1** adopts an 0-D perovskite-like structure. Moreover, organic cations are bonded to anionic clusters through weak N–H···Br hydrogen bonds ($d_{N-Br}=3.4517$ Å; Supporting Information, Figure S3). Although the cationic structure located from the difference Fourier map is refined as an ordered model, the large temperature factors of methyl carbon atoms (Supporting Information, Figure S4) are reminiscent of possible atomic motions, which will favor phase transition in **1**.

Upon heating, the gradually elongated displacement ellipsoids of terminal carbon atoms confirm dynamic hopping-like motions for methyl groups, leading to the disordering of organic cations (Figure 1 b).[17] As temperature increases above 322 K (T_c, Curie temperature, as discussed below), both inorganic moieties and organic cations of **1** become highly disordered. The inorganic framework of $[Sb_2Br_9]^{3-}$ adopts a symmetric configuration, with all the bridging bromide atoms distributed equally between two equivalent octahedra. In contrast to the room temperature structure of **1**, the dioctahedron motif shows a homogenetic restoration that arises from symmetry requirements (Figure 1 b). Moreover, the organic counterparts are refined at two equivalent disordered sites, and the hopping-like motions of methyl groups lead to positive charges carried by nitrogen atoms centered in the mirror planes. Hence, thermally induced order–disorder transformation of inorganic moieties and organic cations leads to the paraelectric-to-ferroelectric phase transition of **1**.

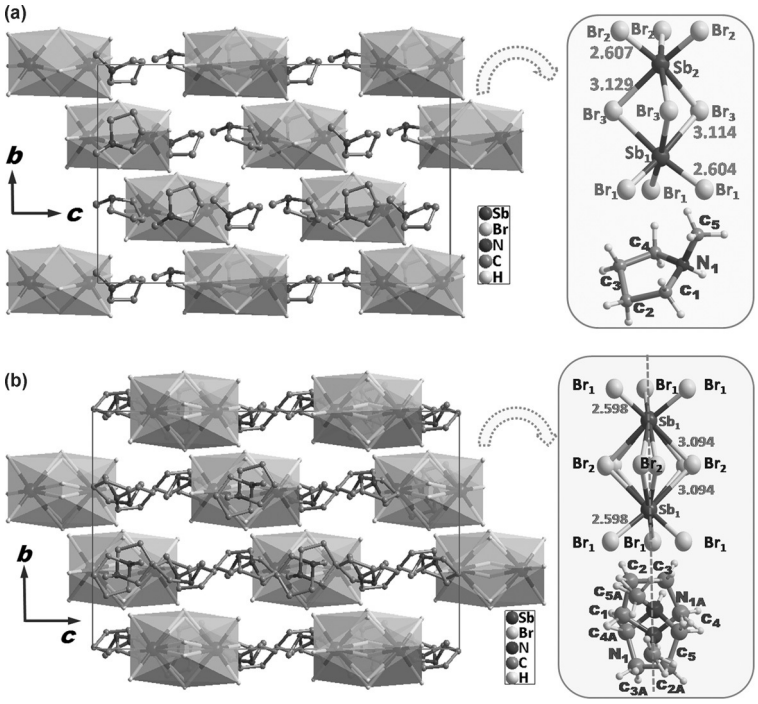

Figure 1. Projections of crystal structures of **1** in a) 293 K and b) 335 K viewed along the *a*-axis. The organic cations at 335 K are highly disordered with two equivalent occupancies, and inorganic dimers also exhibit orientational disordering. The dashed line denotes the crystallographic mirror plane.

The above structural analysis discloses that the crystallographic symmetry of **1** changes from $R\bar{3}c$ (paraelectric phase) to *R*3c (ferroelectric phase) at T_c upon cooling;[18] that is, a ferroelectric phase transition with an Aizu notation of $\bar{3}mF3m$ (Supporting Information, Figure S5). Here, second harmonic generation (SHG) measurement and differential scanning calorimetry (DSC) were performed to confirm symmetry breaking. Variable-temperature SHG effects reveal that **1** undergoes a phase transition from a non-centrosymmetric to a centrosymmetric state, coinciding with sharp heat anomalies in the DSC traces (Figure 2 a). At room temperature, the SHG intensities of **1** are about 0.6 times as large as that of potassium dihydrogen-phosphate ($\chi^{(2)}=0.39\ pm\,V^{-1}$); hence, the quad-

ratic coefficient is estimated to be approximately 0.24 pm V^{-1}. The pronounced dielectric anomaly peaks (Figures 2b; Supporting Information, Figure S6), fit well with the Curie–Weiss law (Figure 2b inset), suggesting the possible ferroelectric activity of **1**.[19] The ferroelectric hysteresis loops at 306 K reveal a saturated spontaneous polarization (P_s) and remnant polarization (P_r) of about 7.6 and 7.3 μC cm^{-2}, respectively (Figure 2c). Such figures are close to that integrated by the pyroelectric currents (Figure 2d), and among the highest values for hybrid ferroelectrics, such as bis(cyclohexylaminium) tetrabromo lead,[20a] (3-pyrrolinium)$CdCl_3$,[20b] and (benzylammonium)$_2PbCl_4$.[21] Figure 2d also shows the temperature-dependent piezoelectric response of **1**; its piezoelectric coefficient d_{33} decreases sharply from 12 pC/N to zero upon heating. As far as we are aware, the large ferroelectric polarization might create a high built-in electrostatic field.[22] Herein, we estimate the local electric field at ferroelectric interfaces from $\mu = \varepsilon_r\varepsilon_0 E$, where μ is charge density, which is related to remnant polarization ($P_r \approx 7.3$ μC cm^{-2}). Dielectric constants (ε_r) are 10–16 at room temperature, and ε_0 denotes the vacuum permittivity. Therefore, the built-in electric field (E) is estimated to be approximately 2×10^5 V mm^{-1}. Such a high electric field might enhance the separation of photon-generated charge carriers and improve the semiconducting behavior of **1**.[23]

Hybrid perovskites based on Sb^{III} are expected to exhibit semiconducting behavior comparable with those of Pb^{II}-based compounds,[16,24] since the Sb^{3+} ion is isoelectronic with Pb^{2+} and these elements also have similar ionic radii and electronegativities. UV/Vis optical diffuse reflectance of **1** shows a gradual absorption edge at about 450 nm (Figure 3a), which is comparable with some perovskite hybrids of $(R\text{-}NH_3)_2PbBr_4$,[20a,25] but slightly smaller than that of $CH_3NH_3PbI_3$.[26] The band gap (E_g) of **1** is estimated to be about 2.76 eV according to the Tauc curve. This value agrees fairly well with our ab initio calculations ($\approx$2.8 eV; Supporting Information), but is much lower than that of some inorganic semiconductors, such as Nb_2O_5, ZnO, and GaN (larger than 3.0 eV).[27] The measured temperature-dependent ac conductivity of **1** (Figure 3b) is consistent with that of the imaginary part (ε'') of the complex dielectric permittivity, which follows the relationship $\sigma_{ac} = \omega\varepsilon''\varepsilon_0$, where ω is the angular frequency and ε_0 is the permittivity of free space.[28] The positive slope of ac conductivity with increasing temperature discloses that **1** should be a semiconductor in the ferroelectric phase.

Photoconductive response is also indicative of the potential semiconducting properties of a material. Photoelectric effects of **1** were studied using a lateral two-probe device architecture (Supporting Information, Figure S8),[29] and weak photoconductivity was observed under UV light (λ = 365 nm, 20 mW cm^{-2}). As shown in Figure 4, the photocurrent increases from 23 pA (dark) to 58 pA (at $V_{bias} = 10$ V) under UV photoexcitation, which is evidence for the semiconducting features of **1**. It is known that light should have enough energy to create electron–hole pairs across the band gap of a semiconductor, or to excite impurities within the band gap; that is, a threshold excitation photon energy is needed. For **1**, the photocurrent becomes quite low with almost negligible levels of photoelectric signals above 450 nm. This can be understood in terms of the decreased number of photoexcited electron–hole pairs while photon energy becomes smaller than its band gap. This indicates that **1** is intrinsically "blind" to visible light.[30] As far as we are aware, **1** might be the first hybrid ferroelectric that is UV sensitive but "blind" to visible light photoelectric effects, although extensive work has been reported on inorganic counterparts.[27] This photoconductivity makes **1** a possible candidate for UV photodetection that is "blind" to visible light.

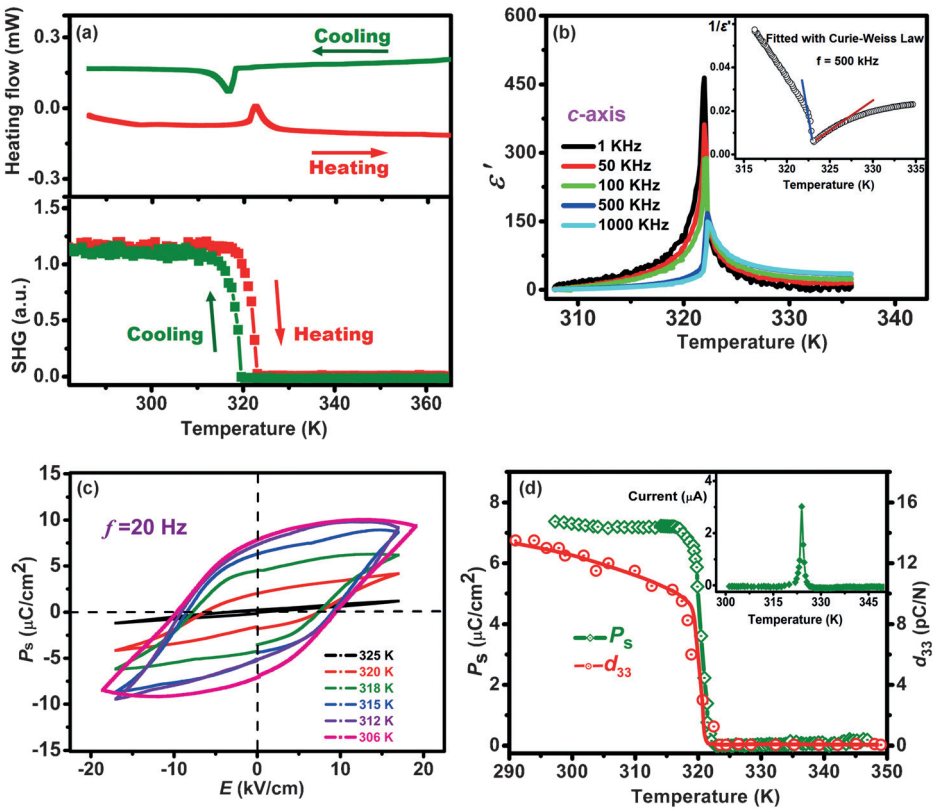

Figure 2. Phase transition and ferroelectric properties of **1**. a) DSC and SHG results. b) Temperature dependence of the real part (ε') of the complex permittivity measured along the *c*-axis. Inset: the plot of $1/\varepsilon'$ vs. temperature in the vicinity of T_c. c) Ferroelectric hysteresis loops measured at 20 Hz. d) Temperature-dependent piezoelectric coefficient d_{33} and spontaneous polarization P_s by integrating pyroelectric current. Inset: the measured pyroelectric current.

To understand the electronic origin of semiconducting properties of **1**, we calculated its band

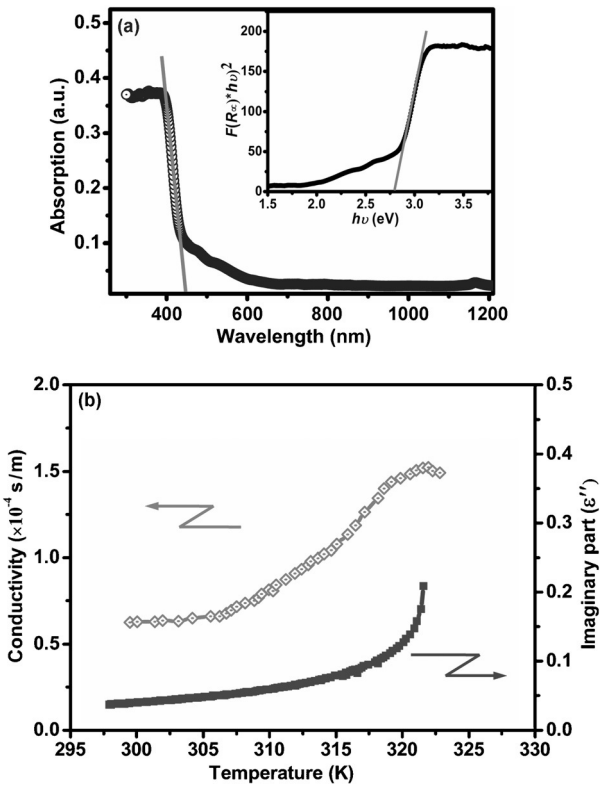

Figure 3. a) Optical diffuse reflectance spectrum for **1**. Inset: the calculated band gap; b) temperature dependence of the conductivity (σ) and imaginary part (ε'') of the complex dielectric permittivity.

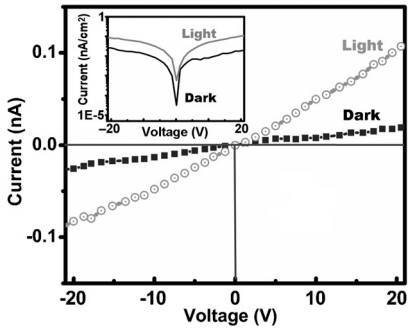

Figure 4. The *I–V* curves performed on single-crystals of **1** under dark and UV light illumination ($\lambda = 365$ nm). Inset: the current density and voltage curves.

structure and energy gap using density functional theory. Figure 5 a shows that both the valence band maximum (VBM) and conduction band minimum (CBM) are located at the *G* point, and the calculated band gap is about 2.8 eV. Additionally, the partial density of states (PDOS) reveal that H 1s states overlap fully with C 2s and *N* 2s2p states in the range from −15 to −2.5 eV. For the 0-D inorganic moieties, quite strong overlap is observed between Sb s/p and Br s/p in the conduction region. The flat VBM bands mainly result from the nonbonding states of Br 4p, while the intensive CBM bands originate from Sb 5p states. Such coupling reveals that the band gap of **1** is determined by the electronic structure of the inorganic 0-D clusters, resembling some tin-, lead-

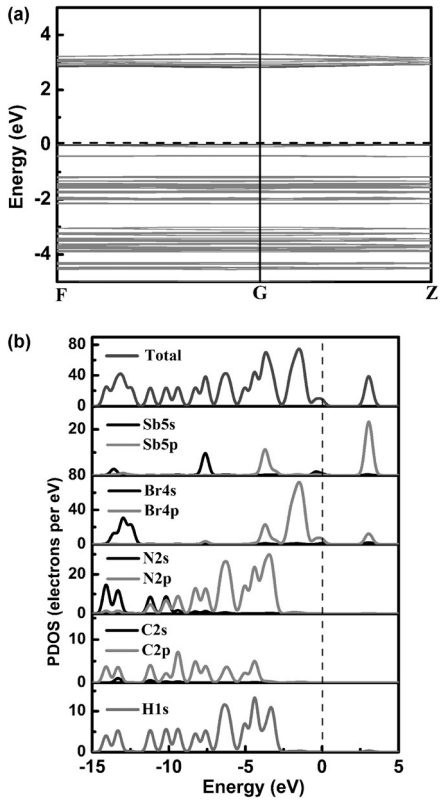

Figure 5. a) The calculated band structure and b) PODS of **1**.

based,[31] and Sb^{III}-based perovskite hybrids.[16b] This result indicates that the energy gap may be confidently tuned by chemical tailoring.[32]

In summary, we have successfully reported a lead-free semiconducting hybrid ferroelectric, adopting a 0-D perovskite structure based on the distorted $SbBr_6$ octahedra, which shows large spontaneous polarization of about 7.6 $\mu C\,cm^{-2}$. It is found that order–disorder transformation of organic moieties makes a great contribution to its ferroelectricity, while the inorganic 0-D perovskite framework determines the semiconducting properties. Since low-dimensional perovskite hybrids benefit from structural variability and tunability, a fine tuning of inorganic and/or organic components will optimize the electronic and optical properties. This study opens up broad opportunities and innovative applications for perovskite hybrids, especially for environmentally benign semiconducting ferroelectrics.

Acknowledgements

This work was supported by NSFC (21525104, 91422301, 21373220, 51402296, 21571178, 51502288, 51502290 and 21301172), the Strategic Priority Research Program of the Chinese Academy of Sciences (XDB20000000), the NSF for Distinguished Young Scholars of Fujian Province (2014J06015), Youth Innovation Promotion of CAS (2014262), and "Chunmiao Projects" of Haixi Institute of CAS (CMZX-2013-002). A.Z. thanks the CAS-TWAS President's fellowship of UCAS.

Keywords: band gap · ferroelectrics · perovskite hybrids · phase transitions · semiconducting properties

How to cite: *Angew. Chem. Int. Ed.* **2016**, *55*, 11854–11858
Angew. Chem. **2016**, *128*, 12033–12037

[1] H. Zhu, Y. Fu, F. Meng, X. Wu, Z. Gong, Q. Ding, M. V. Gustafsson, M. T. Trinh, S. Jin, X. Y. Zhu, *Nat. Mater.* **2015**, *14*, 636.

[2] C. R. Kagan, D. B. Mitzi, C. D. Dimitrakopoulos, *Science* **1999**, *286*, 945.

[3] a) M. M. Lee, J. Teuscher, T. Miyasaka, T. N. Murakami, H. J. Snaith, *Science* **2012**, *338*, 643; b) F. Hao, C. C. Stoumpos, R. P. H. Chang, M. G. Kanatzidis, *J. Am. Chem. Soc.* **2014**, *136*, 8094; c) I. C. Smith, E. T. Hoke, D. Solis-Ibarra, M. D. McGehee, H. I. Karunadasa, *Angew. Chem. Int. Ed.* **2014**, *53*, 11232; *Angew. Chem.* **2014**, *126*, 11414; d) N. J. Jeon, J. H. Noh, Y. C. Kim, W. S. Yang, S. Ryu, S. I. Seok, *Nat. Mater.* **2014**, *13*, 897; e) A. Sharenko, M. F. Toney, *J. Am. Chem. Soc.* **2016**, *138*, 463; f) S. Pang, Y. Zhou, Z. Wang, M. Yang, A. R. Krause, Z. Zhou, K. Zhu, N. P. Padture, G. Cui, *J. Am. Chem. Soc.* **2016**, *138*, 750.

[4] C. S. Ponseca, Jr., T. J. Savenije, M. Abdellah, K. Zheng, A. Yartsev, T. Pascher, T. Harlang, P. Chabera, T. Pullerits, A. Stepanov, J.-P. Wolf, V. Sundström, *J. Am. Chem. Soc.* **2014**, *136*, 5189.

[5] S. D. Stranks, G. E. Eperon, G. Grancini, C. Menelaou, M. J. P. Alcocer, T. Leijtens, L. M. Herz, A. Petrozza, H. J. Snaith, *Science* **2013**, *342*, 341.

[6] A. Stroppa, D. Sante, P. Barone, M. Bokdam, G. Kresse, C. Franchini, M. H. Whangbo, S. Picozzi, *Nat. Commun.* **2014**, *5*, 5900.

[7] a) J. M. Frost, K. T. Butler, F. Brivio, C. H. Hendon, M. van Schilfgaarde, A. Walsh, *Nano Lett.* **2014**, *14*, 2584; b) C. C. Stoumpos, C. D. Malliakas, M. G. Kanatzidis, *Inorg. Chem.* **2013**, *52*, 9019; c) A. Stroppa, C. Quarti, F. D. Angelis, S. Picozzi, *J. Phys. Chem. Lett.* **2015**, *6*, 2223.

[8] H. Huang, *Nat. Photonics* **2010**, *4*, 134.

[9] Y. Kutes, L. Ye, Y. Zhou, S. Pang, B. D. Huey, N. P. Padture, *J. Phys. Chem. Lett.* **2014**, *5*, 3335.

[10] a) H. Lu, C. W. Bark, D. E. Ojos, J. Alcala, C. B. Eom, G. Catalan, A. Gruverman, *Science* **2012**, *336*, 59; b) J. F. Scott, *Science* **2007**, *315*, 954; c) H.-Y. Ye, W.-Q. Liao, C.-L. Hu, Y. Zhang, Y.-M. You, J.-G. Mao, P.-F. Li, R.-G. Xiong, *Adv. Mater.* **2016**, *28*, 2579.

[11] a) D. B. Mitzi, *J. Chem. Soc. Dalton Trans.* **2001**, 1; b) G. Kieslich, S. Sun, A. K. Cheetham, *Chem. Sci.* **2014**, *5*, 4712; c) G. Kieslich, S. Sun, A. K. Cheetham, *Chem. Sci.* **2015**, *6*, 3430.

[12] L. Liang, L. Wencong, C. Nianyi, *J. Phys. Chem. Solids* **2004**, *65*, 855.

[13] a) A. Kallel, J. W. Bats, *Acta Crystallogr. Sect. C* **1985**, *41*, 1022; b) L. Latanowicz, W. Medycki, R. Jakubas, *J. Phys. Chem. A* **2005**, *109*, 3097; c) W. Zhang, R.-G. Xiong, *Chem. Rev.* **2012**, *112*, 1163.

[14] a) L. Pauling, *The Nature of the Chemical Bond*, Cornell University Press, Ithaca, NY, **1960**; b) R. Shannon, *Acta Crystallogr. Sect. A* **1976**, *32*, 751.

[15] a) M. Wojtaśa, R. Jakubasa, Z. Ciunika, W. J. Medyckib, *J. Solid State Chem.* **2004**, *177*, 1575; b) H. Ishihara, K. Watanabe, A. Iwata, K. Yamada, Y. Kinoshita, T. Okuda, V. G. Krishnan, S.-Q. Dou, A. Weiss, *Z. Naturforsch. A* **1992**, *47*, 65.

[16] a) B. Saparov, F. Hong, J.-P. Sun, H.-S. Duan, W. Meng, S. Cameron, I. G. Hill, Y. Yan, D. B. Mitzi, *Chem. Mater.* **2015**, *27*, 5622; b) B. Saparov, D. B. Mitzi, *Chem. Rev.* **2016**, *116*, 4558.

[17] a) H.-Y. Ye, Q. H. Zhou, X. H. Niu, W.-Q. Liao, D.-W. Fu, Y. Zhang, Y.-M. You, J. Wang, Z.-N. Chen, R.-G. Xiong, *J. Am. Chem. Soc.* **2015**, *137*, 13148; b) Y. Zhang, W.-Q. Liao, D.-W. Fu, H.-Y. Ye, Z.-N. Chen, R.-G. Xiong, *J. Am. Chem. Soc.* **2015**, *137*, 4928.

[18] Crystal data for **1:** $T = 335$ K, $C_{15}H_{36}Br_9N_3Sb_2$, $M_r = 1221.16$, trigonal, $R\bar{3}c$, $a = 15.9951(4)$, $c = 23.1124(7)$ Å, $V = 5120.9(2)$ Å^3, $Z = 6$, $\rho_{cal.} = 2.376$ g cm^{-3}, $S = 1.097$, $R_1(I > 2\sigma(I)) = 0.0504$, $wR_2(I > 2\sigma(I)) = 0.1491$; $T = 293$ K, trigonal, $R3c$, $a = 15.6943(2)$, $c = 23.5279(4)$ Å, $V = 5018.77(12)$ Å^3, $Z = 6$, $\rho_{cal.} = 2.424$ g cm^{-3}, $S = 1.079$, $R_1(I > 2\sigma(I)) = 0.0798$, $wR_2\ (I > 2\sigma(I)) = 0.1871$.

[19] M. E. Lines, A. M. Glass, *Principles and Applications of Ferroelectrics and Related Materials*, Oxford University Press, New York, **2001**.

[20] a) Z. Sun, X. Liu, T. Khan, C. Ji, M. A. Asghar, S. Zhao, L. Li, M. Hong, J. Luo, *Angew. Chem. Int. Ed.* **2016**, *55*, 6545; *Angew. Chem.* **2016**, *128*, 6655; b) H.-Y. Ye, Y. Zhang, D.-W. Fu, R.-G. Xiong, *Angew. Chem. Int. Ed.* **2014**, *53*, 11242; *Angew. Chem.* **2014**, *126*, 11424.

[21] R. C. Naber, C. Tanase, P. W. M. Blom, G. H. Gelinck, A. W. Marsman, F. J. Touwslager, S. Setayesh, D. W. Deleeuw, *Nat. Mater.* **2005**, *4*, 243.

[22] a) S. Kundu, M. Clavel, P. Biswas, B. Chen, H.-C. Song, P. Kumar, N. N. Halder, M. K. Hudait, P. Banerji, M. Sanghadasa, S. Priya, *Sci. Rep.* **2015**, *5*, 12415; b) W.-Q. Liao, Y. Zhang, C.-L. Hu, J.-G. Mao, H.-Y. Ye, P.-F. Li, S. D. Huang, R.-G. Xiong, *Nat. Commun.* **2015**, *6*, 7388.

[23] X. Wang, P. Wang, J. Wang, W. Hu, X. Zhou, N. Guo, H. Huang, S. Sun, H. Shen, T. Lin, M. Tang, L. Liao, A. Jiang, J. Sun, X. Meng, X. Chen, W. Lu, J. Chu, *Adv. Mater.* **2015**, *27*, 6575.

[24] a) E. Y. Peresh, V. I. Sidei, O. V. Zubaka, I. P. Stercho, *Inorg. Mater.* **2011**, *47*, 208; b) D. B. Mitzi, *Inorg. Chem.* **2000**, *39*, 6107.

[25] D. G. Billing, A. Lemmerer, *CrystEngComm* **2009**, *11*, 1549.

[26] A. Kojima, K. Teshima, Y. Shirai, T. Miyasaka, *J. Am. Chem. Soc.* **2009**, *131*, 6050.

[27] a) H. Chen, K. Liu, L. Hu, A. A. Al-Ghamdi, X. Fang, *Mater. Today* **2015**, *18*, 493; b) L. Hu, L. Wu, M. Liao, X. Fang, *Adv. Mater.* **2011**, *23*, 1988.

[28] a) W. Kuang, S. O. Nelson, *Trans. ASAE* **1998**, *41*, 173; b) F. Kremer, A. Schönhals, *Broadband Dielectric Spectroscopy*, Springer, Berlin, **2002**.

[29] a) Y. Yuan, Z. Xiao, B. Yang, J. Huang, *J. Mater. Chem. A* **2014**, *2*, 6027; b) R. Moubah, O. Rousseau, D. Colson, A. Artemenko, M. Maglione, M. Viret, *Adv. Funct. Mater.* **2012**, *22*, 4814.

[30] W. Tian, C. Zhang, T. Zhai, S.-L. Li, X. Wang, J. Liu, X. Jie, D. Liu, M. Liao, Y. Koide, D. Golberg, Y. Bando, *Adv. Mater.* **2014**, *26*, 3088.

[31] a) I. Borriello, G. Cantele, D. Ninno, *Phys. Rev. B* **2008**, *77*, 235214; b) W.-J. Yin, J.-H. Yang, J. Kang, Y. Yan, S.-H. Wei, *J. Mater. Chem. A* **2015**, *3*, 8926.

[32] E. Mosconi, A. Amat, M. K. Nazeeruddin, M. Grätzel, F. D. Angelis, *J. Phys. Chem. C* **2013**, *117*, 13902.

Received: June 22, 2016
Published online: August 22, 2016

